



Crustal thickness and structural pattern evaluation of Sinai Peninsula using three-dimensional density modeling with aeromagnetic and earthquake data

Gaber M. Gaber¹ · Salah Saleh² · Mostafa Toni¹

Received: 8 October 2021 / Accepted: 13 February 2022 / Published online: 10 March 2022
© The Author(s) 2022

Abstract

The Sinai Peninsula is a subplate located between the African and Arabian plates. It is an important subplate in the world; however, this region is poorly understood because of the shortage of geophysical data. Thus, this study focuses on built a three-dimensional (3D) high-resolution forward model of the crustal thickness with a new tectonic model and structural evaluation of the Sinai Peninsula to understand this area tectonically and determine its lithospheric and crustal thicknesses. Qualitative and quantitative interpretations of Bouguer gravity, reduced-to-the-pole (RTP) aeromagnetic, and earthquake data are explained to achieve the goals of this study. Two-dimensional (2D) interactive sequential modeling of gravity data is performed along with some well-selected profiles with existing crustal layer depth points from previous works in the studied region. Seventeen 2D models are constructed and used to determine the basement, Conrad (lower crust boundary), and Moho (upper mantle boundary) depths and to build a 3D model. Accuracy of the 3D built model is evaluated by extracting observed, calculated, and residual gravity anomaly maps. The results show that the basement rocks appear on the surface in the South of Sinai and deepen (down to 4.5 km) toward the North. The Conrad surface varies approximately from 16 km (in the northeast and southwest of Sinai) to 22.8 km (in the southeast). The Moho surface depth (i.e., crustal thickness) varies approximately from 28.8 to 34.2 km, and it deepens toward the northeastern and southwestern parts of Sinai. A tentative basement structure map is constructed from the horizontal gradient (H-gradient) filter and the 3D Euler deconvolution of the Bouguer gravity and RTP aeromagnetic data. Correlation between the geological background of the study area and the obtained results suggests that the Sinai Peninsula is tectonically active, mainly in its southern portion due to the tectonic movements along the Gulf of Suez and the Gulf of Aqaba. The crustal thickness increases southward and thins northward.

Keywords Sinai Peninsula · 3D density modeling · Crustal thickness · Bouguer anomaly · Aeromagnetic data · Earthquake data

Introduction

The Sinai Peninsula is a subplate that has been interacting over recent geological time with the southeastern Mediterranean plate. The central and northern parts of the Sinai

subplate are characterized by a sequence of NE–SW-trending anticline mountains, and a limestone plateau dominates. Basement rocks of Precambrian age dominate the southern part of the Sinai Peninsula and reach 2640 m at Gebel (i.e., mountain) Katharina (Said 1962).

Reduced-to-the-pole (RTP) aeromagnetic data together with Bouguer gravity data have been used to detect the structural trends and crustal thickness (basement surface and Conrad and Moho discontinuities) in the Sinai Peninsula. Different processing techniques have been adopted for gravity and aeromagnetic data. The regional–residual separation technique has been applied to RTP aeromagnetic and Bouguer anomaly maps to define the deep and shallow tectonic trends in the study area that affect the basement surface and the overlying sedimentary layer. The basement

Edited by Prof. Ivana Vasiljević (ASSOCIATE EDITOR) / Prof. Michał Malinowski (CO-EDITOR-IN-CHIEF).

✉ Gaber M. Gaber
Gaber.magdy@science.helwan.edu.eg

¹ Geology Department, Faculty of Science, Helwan University, Ain Helwan, Cairo, Egypt

² National Research Institute of Astronomy and Geophysics (NRIAG), Helwan, Cairo, Egypt

depth was estimated using the spectral analysis technique along with 17 2D Bouguer gravity profiles. A 3D gravity model was built to estimate the crustal thickness in the Sinai region. Furthermore, a horizontal gradient (H-gradient) filter and the 3D Euler deconvolution technique of Bouguer and RTP aeromagnetic data were used in structural evaluations within the investigated region. Earthquake data in terms of location, depth, and magnitude was also used to trace the structural activity in the Sinai Peninsula.

Several studies (e.g., Ginzburg et al. 1981; Marzouk 1988; Saleh et al. 2006; Abdelwahed et al. 2013; Mohamed et al. 2016; Corchete et al. 2017) have been performed to identify the crustal thickness in the Sinai Peninsula. They used different geophysical methods (e.g., seismic refraction, gravity, and magnetic); however, they could not completely estimate the depths of the basement surface and the discontinuities of Conrad and Moho. Therefore, the results of the current work and those of previous studies were integrated to develop a 3D high-resolution density model of the crustal

thickness and a structural map for the Sinai Peninsula to understand the tectonism of the region.

Geologic and tectonic settings

Precambrian basement rocks exist in Southern Sinai, parallel to the Gulf of Suez and the Gulf of Aqaba. Sediments of Mesozoic to Tertiary age exist in the central part of Sinai. Furthermore, the Northern Sinai topography comprises low alluvial plains that have a thick sedimentary cover and are cracked by Mesozoic domes and anticlines (Syrian Arc) (Said 1962).

The Sinai Peninsula has northern and northwestern transgressions (Shata 1955). Most common occurrences in the Cretaceous and Eocene (as observed in the central part of Sinai, South Yelleg) have been recorded, and they advance to the Jurassic shield (i.e., East Maghara, North Maghara, Northern Falling and Rafah) (Fig. 1). During the post-Eocene period, many marine transgressions were

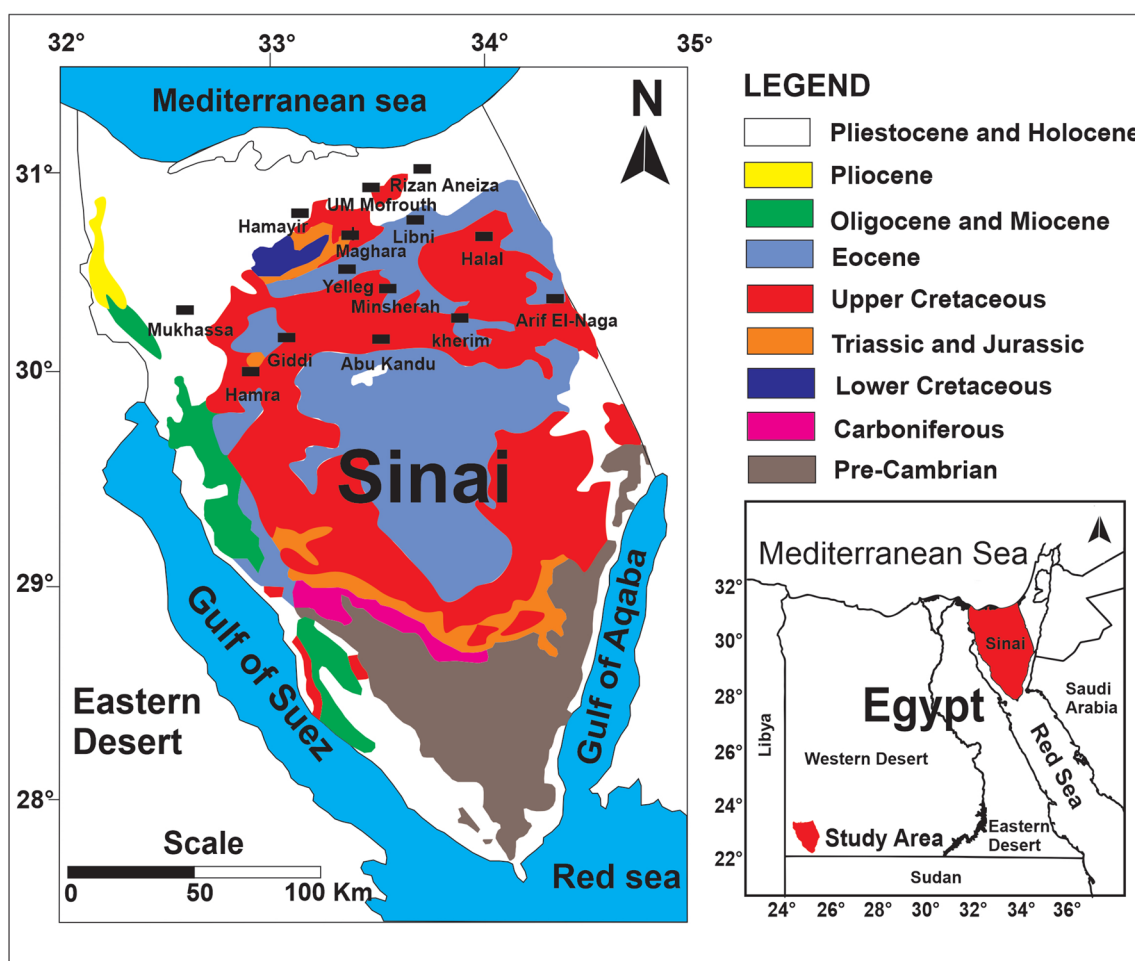


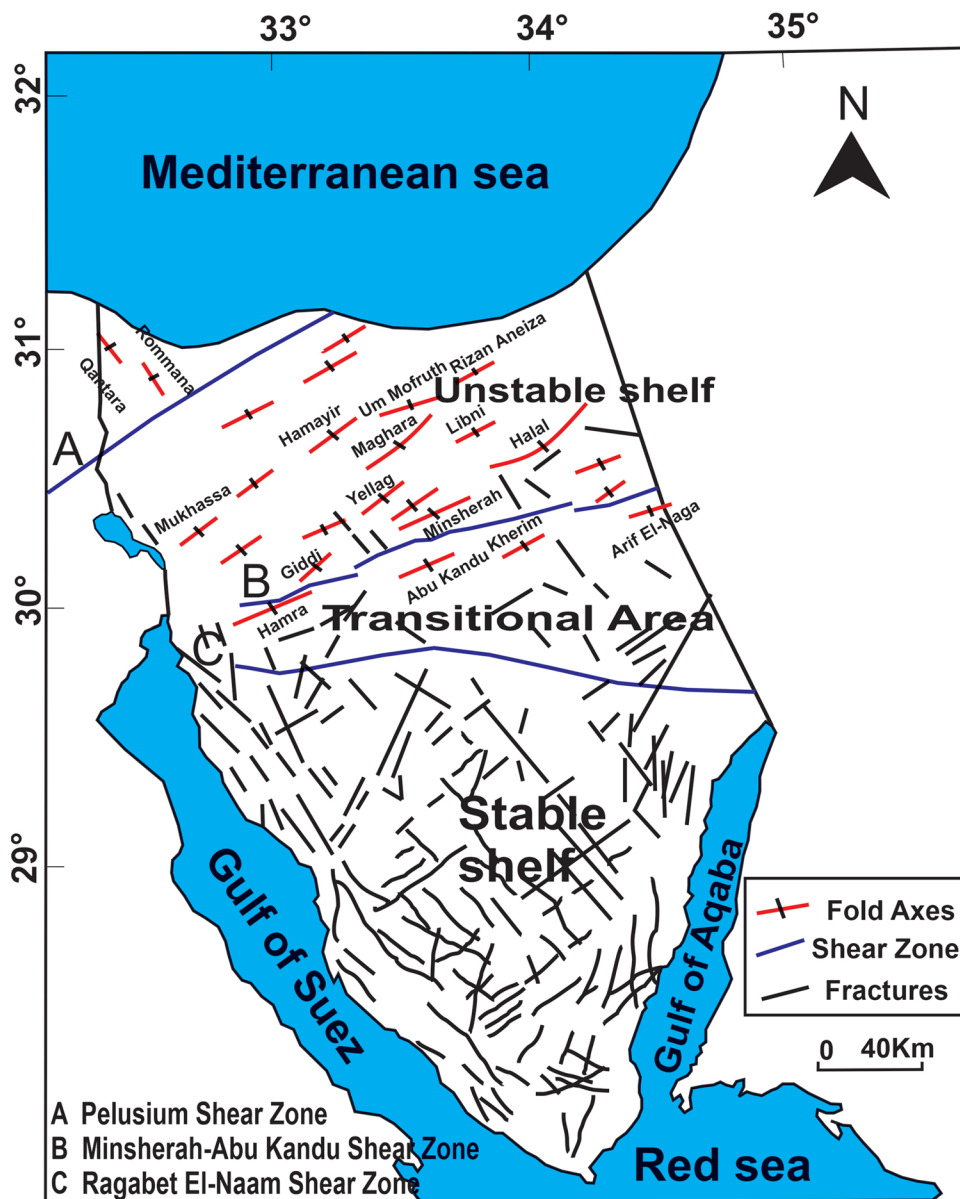
Fig. 1 Simplified geological map of the Sinai Peninsula (modified after Omara 1972; Kora 1995)

received in Sinai (in the Mediterranean and then in the western offshore regions). The geological map illustrated in Fig. 1 shows that the Sinai Peninsula has rock units of different ages (e.g., Triassic, Jurassic, Cretaceous, and Tertiary).

Northern Sinai is almost flat except the southeastern portion of the Maghara anticline, which is NE–SW trending and features an elevated area (Abu El-Ata et al. 1991). The southern portion of Northern Sinai is a separate line of elliptical NE-trending ridges with elongated depressions between them (e.g., Gebel Yelleg and Gebel Halal). Furthermore, smaller crests exist such as Gebel Libni and Gebel Minsherah (Fig. 1) (Shata 1956; El-Kerdany 1962; Moustafa and Khalil 1987, 1990).

The Northern Sinai area has alternating faulted domes, anticlines, and synclines. The Syrian Arc refers to anticlinal and synclinal folds extending from Jordan (west) to Syria (east) (Said 1962). In Northern Sinai, the Pelusium shear line (Fig. 2) represents the major and the oldest regional structural pattern with NNE–SSW trend (Neev et al. 1973). Before bending northward, the eastern part of the Pelusium line extends over the North Sinai continental shelf, thus creating a series of striking faults between the NNE and SSW directions, following the Palestinian continental direction. The Sinai subplate is subdivided into various tectonic blocks and basins (Meshref 1989; Meshref and Hammouda 1990). South of the Pelusium axis, the Mesozoic hinge divides the northernmost block into two sub-blocks (Northern Mesozoic hinge block and Southern Mesozoic hinge block). Thrusting

Fig. 2 A map showing distribution of the tectonic components in Sinai Peninsula (modified after Neev 1975)



and folding originating from the Oligo-Miocene period are dominant in the northern block.

The existence of basement rocks in Southern Sinai is distinguished by the presence of volcano-sedimentary rocks and post-collisional calc-alkaline and alkaline granites (Khalaf et al. 1994; El Nashar et al. 2012; Sherif et al. 2013; Ghoneim et al. 2015). The El Qaa basin, which has the same extension as that of the Gulf of Suez, features a Cenozoic sedimentary section (Fig. 1). Moreover, the NW–SE-trending fault system of the Gulf of Suez and the NNE–SSW-trending fault system of the Gulf of Aqaba impact the southern part of Sinai (Fig. 2).

Data sources

The Bouguer anomaly map shown in Fig. 3A was compiled by the Egyptian General Petroleum Corporation (EGPC 1985); the contour interval (CI) is 1 mGal, and the scale is 1:100,000. The aeromagnetic map shown in Fig. 3B, with a 1 km altitude elevation along parallel flight lines and a scale of 1:100,000, it was prepared by EGPC (1990) as well. The spacing between flight lines was 1 km (in the NE–SW direction) and 10 km (in NW–SE direction). The geomagnetic parameters required for applying the RTP filter

were determined using an IGRF model of the research area. The earthquake data including the focal depth distribution (Fig. 4A) and magnitude distribution (Fig. 4B), was collected from the Egyptian National Seismic Network (ENSN) database from stations distributed along the Sinai region (Fig. 5) for the time span (1998–2018).

Data analysis and interpretations

Bouguer anomaly

Figure 3A shows the Sinai Peninsula's Bouguer anomaly data, which may be subdivided into two main parts. The *first part* consists of positive anomalies (up to 15 mGal) in the central and northwestern parts of Sinai. A high gravitational field is distinguished by a decrease in the crustal thickness in the North and West directions. The *second part* is the negative anomalies in the southeastern part of Sinai, which vary between -73 and -108 mGal and represent a low gravitational field where the crust thickens increases.

In this work, the Bouguer anomalies were separated into their regional and residual components via wavenumber filtering. The cutoff wavenumber was selected by computing the radial power spectrum and by identifying the

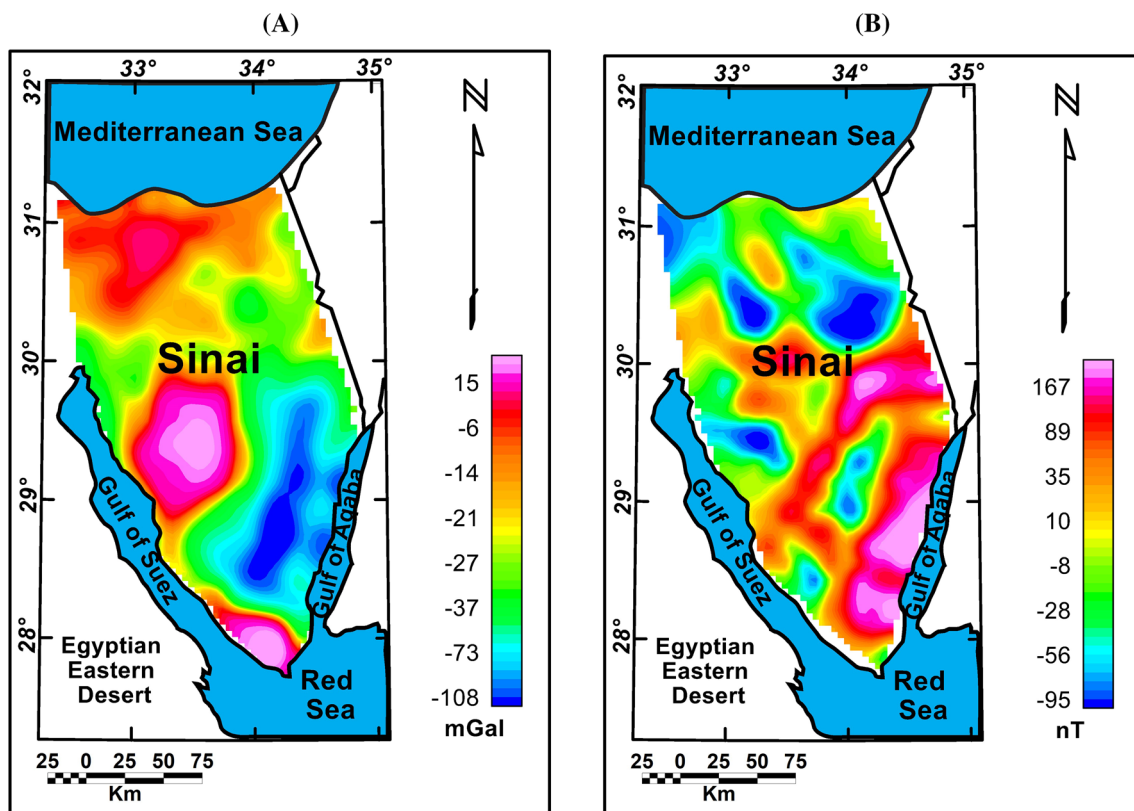


Fig. 3 A Bouguer anomaly map, and B RTP aeromagnetic map of the Sinai Peninsula

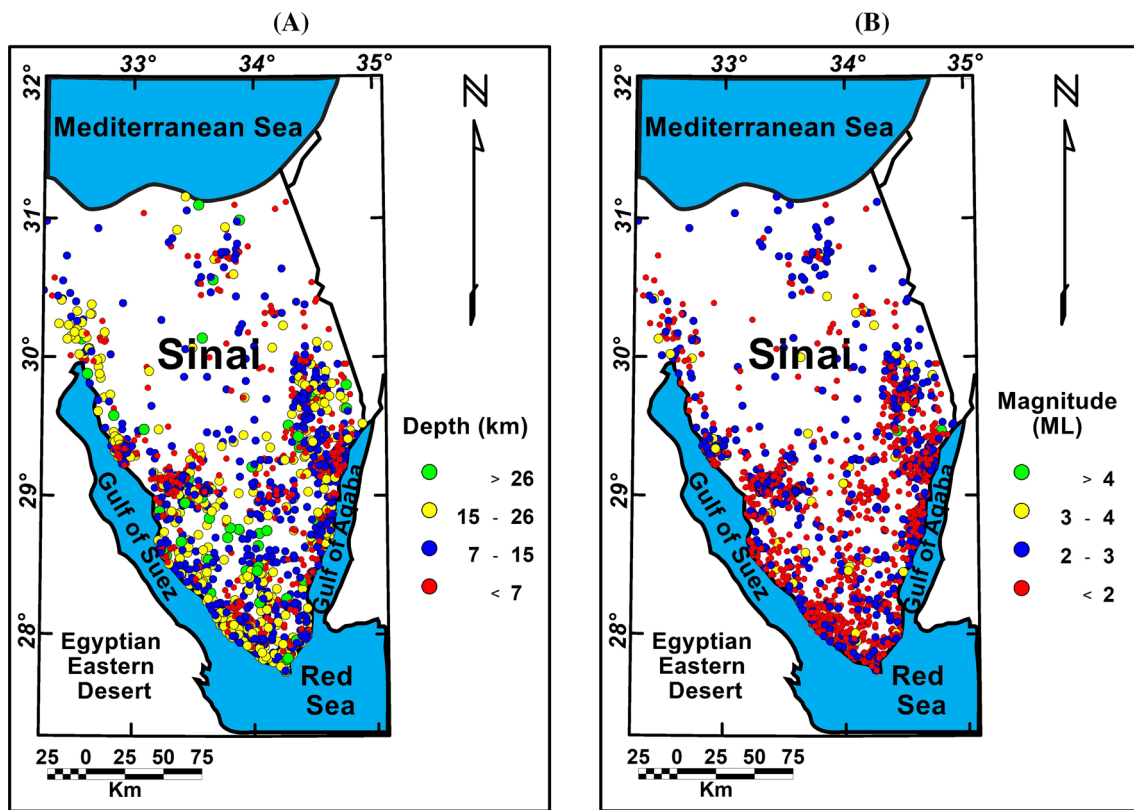


Fig. 4 Distribution of earthquake foci in the Sinai Peninsula during the time span (1998–2018). **A** Focal depth distribution, and **B** Magnitude distribution

wavenumber at which the spectrum changes its slope (0.023 cycles/km) (Fig. 6A).

The low-pass gravitational magnitude ranges between above + 12 mGal (in the northern and middle parts of the study area) and below – 104 mGal (in the southeastern part). The low-pass gravitational map, which represents anomalies with different shapes, directions, and extensions, shows the long-wavelength Bouguer anomalies (regional). Figure 7A depicts low-pass filter anomalies; the significant anomalies are positive in the northern and central parts, representing a thin crust and a shallow Moho depth. Meanwhile, in the southeastern anomalies, the negative values increase where the crust thickens, and the Moho surface depth is deep. Small anomalies were obtained from the high-pass filter. These anomalies follow the Sinai area's major structural patterns (NE–SW and NW–SE). The main fault patterns (NW–SE and NE–SW) are still visible in the Bouguer anomaly map, implying that the dominant underground fault trends spread to shallow depths.

The high-pass filter for the Bouguer anomaly map is illustrated in Fig. 7B and features different forms and closed anomalies. The symmetry of these forms in the North is almost rounded, implying that the body is a plug. Anomalies with extended shapes appear at different parts in Sinai, and

the possible source may be a dyke, with the strike indicating an elongated direction.

The high-pass filter magnitude of the gravity fields ranges between above + 4 mGal and below – 6 mGal. The positive gravity anomalies are mostly through shallow, dense bodies or raised surfaces. The negative gravity values in the northern part of Sinai reflect a thick sedimentary cover (Fig. 7B). In the southeastern part of Sinai, the negative gravity values are related to the strain of the Gulf of Suez and the Gulf of Aqaba (Fig. 7B).

RTP aeromagnetic data

The RTP filter is intended to simplify the interpretation of total magnetic field data, depending on the magnetization source. Thus, magnetic anomalies are linked to their sources, and convenient and reliable interpretations can be obtained. Figure 3B shows the RTP aeromagnetic map, where the magnitude of the magnetic field varies from – 95 to 167 nT. The highest magnetic intensity (up to + 167 nT) is recorded in the South and the center of Sinai, where high-magnetization basement rocks are located.

The magnetic anomalies are mostly elongated oval, and some are almost round. In the center and in the South of

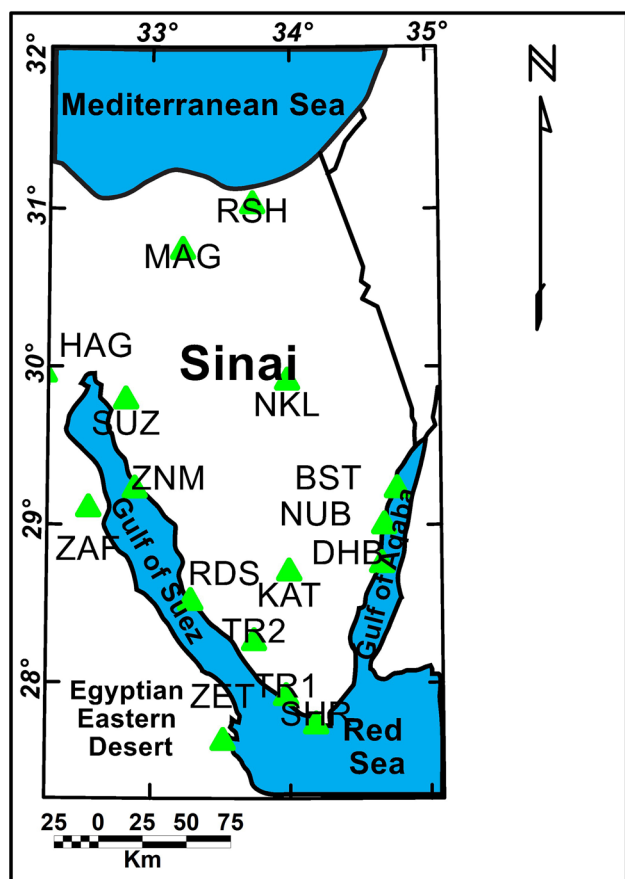


Fig. 5 Distribution of ENSN's stations in and around the Sinai Peninsula

Sinai, an essential magnetic anomaly represented by oval-shaped Tertiary volcanic and granitic intrusions is observed. Some small, circular anomalies (positive and negative) show uplifts and local basins. The main magnetic anomalies patterns are observed along with E–W, NE–SW, and NW–SE trends, these patterns are parallel to the direction of the region's geological and structural trends. There are sharp anomalies between the southern part of Sinai and some parts in the North; basement rocks are deeper in the central part of Northern Sinai.

In gravity analysis, deep and shallow anomaly maps have been separated via the application of wavenumber filtering. The cutoff wavenumber was selected by computing the radial power spectrum and by identifying the wavenumber at which the spectrum changes its slope (0.01 cycles/km) (Fig. 6B). The low-pass anomaly map (Fig. 8A) represents the deep sources and structures of the basement surface, while the high-pass anomaly map (Fig. 8B) represents shallow structural features. The high-pass map and the RTP aeromagnetic map reveal the same resemblance and interpretation.

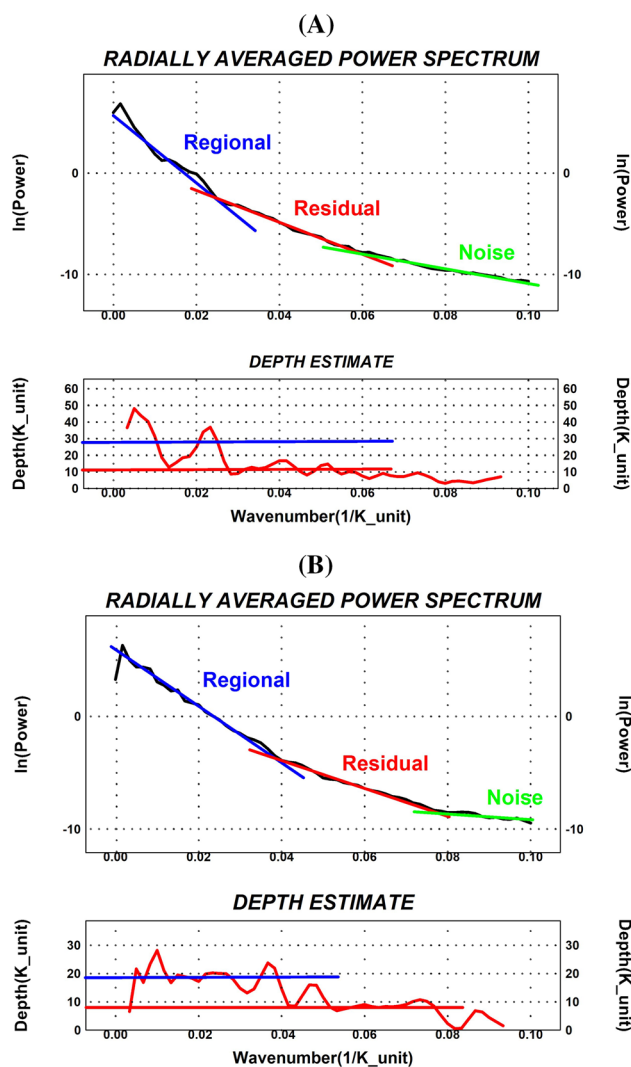


Fig. 6 Radially Power spectral analysis from A Bouguer data, and B RTP aeromagnetic data

Edge detection

3D Euler deconvolution

Thompson (1982) applied the 3D Euler technique to profile data, and this method was subsequently advanced to gridded data by Reid et al. (1990). The 3D Euler process is used to estimate the subsurface characteristics, e.g., fault positions and depths, geological contacts, lineaments, dykes, and sills. Therefore, it requires information about causal bodies, which may be obtained by defining the structural index (SI) (Salem et al. 2008; Eweis et al. 2021). Depending on source geometry, the SI is defined as the rate of field change. In the present study, the 3D Euler technique has been used for magnetic fields and gravity data to identify positions and depth values in the studied area for various lineaments and faults.

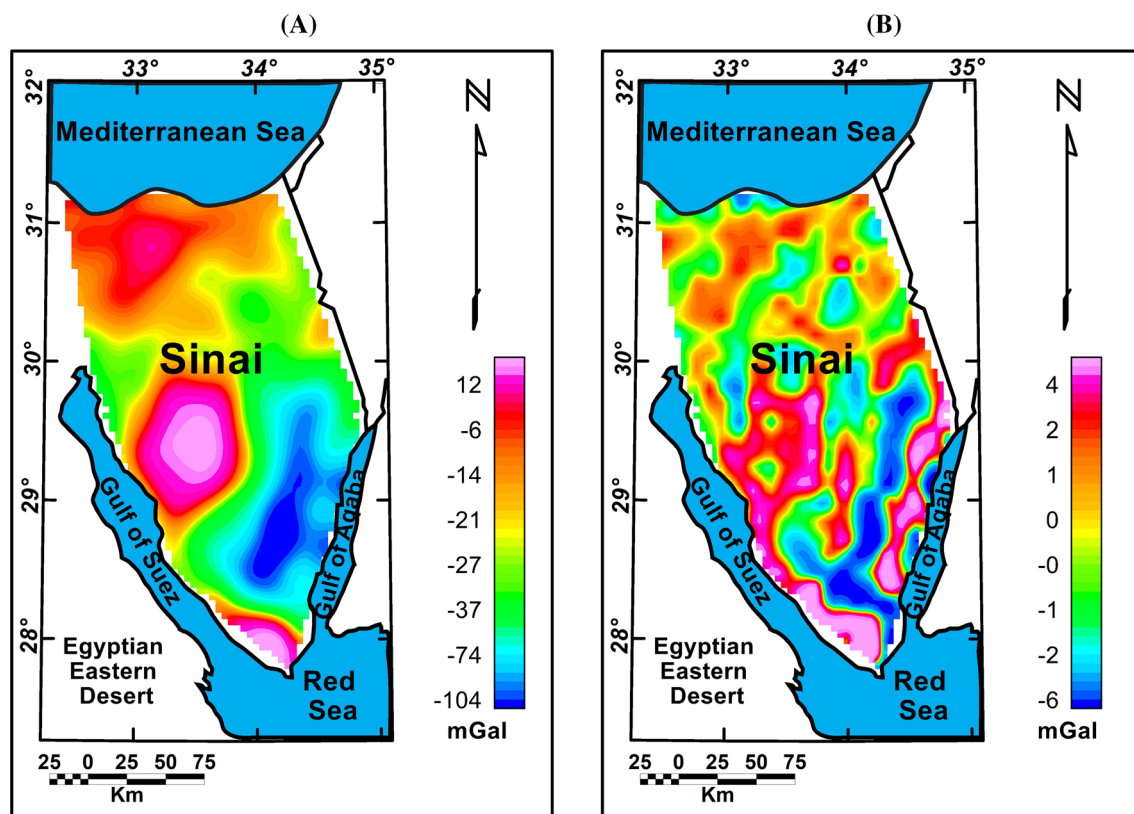


Fig. 7 Filtered Bouguer images. **A** Regional low-pass filter (cutoff wavenumber=0.023 cycle/km). **B** Residual high-pass filter (cutoff wavenumber=0.023 cycle/km)

The Euler's solutions were applied to the Bouguer and RTP aeromagnetic maps of the area under investigation, and the obtained solutions for both data types are illustrated in Fig. 9. The use of $SI = 1$ for the Bouguer map (Fig. 9A) produced good solutions for the lineaments, geological contacts, faults, dykes, and sills, whereas the use of $SI = 0.5$ for the RTP aeromagnetic map (Fig. 9B) gave good solutions for the lineaments, geological contacts, and faults.

A tentative basement structural map (Fig. 10) showing the distribution of fractures along the Sinai region was extracted from the 3D Euler map compiled from the RTP aeromagnetic and Bouguer data. The shallow features are represented by magnetic data, while the deep features are represented by gravity data. The direction of primary trend shown in the Rose diagram is NW–SE (Fig. 10).

H-gradient anomaly maps

The H-gradient technique is used intensively to interpret Bouguer and RTP aeromagnetic data. For the study area, the H-gradient map of Bouguer anomaly data (Fig. 11A) shows sharp, curved NW and NE lines parallel to the Gulf of Suez and the Gulf of Aqaba. These lines represent the faults that influence the tectonics of the area. In this study, the

H-gradient map computed from the RTP aeromagnetic data is depicted in Fig. 11B. Significant faults in the ENE–WSE, NW, and NE directions may dissect the region. The most important result is that the locations of major faults are parallel to the geological and lithological boundaries of the Sinai region (see Fig. 2).

The tentative basement structural map extracted from the H-gradient filter of the Bouguer and RTP aeromagnetic data is shown in Fig. 12. The shallow features are represented by the magnetic data, while the deep features are represented by the gravity data. The directions of primary trends shown in the Rose diagrams (Fig. 12) are NW–SE and NE–SW.

3D gravity forward model

The Bouguer data were sequentially modeled (Fig. 3A) instead of individually modeling each data type, and this provided constrained interpretation results. The density contrast of different rocks was modeled among Bouguer data. Forward modeling describes parameters and anomaly calculation (Bhattacharyya 1965). Similarly, gravity modeling is an important method of studying crustal thickness. The low-pass filter anomalies of Bouguer data are clear

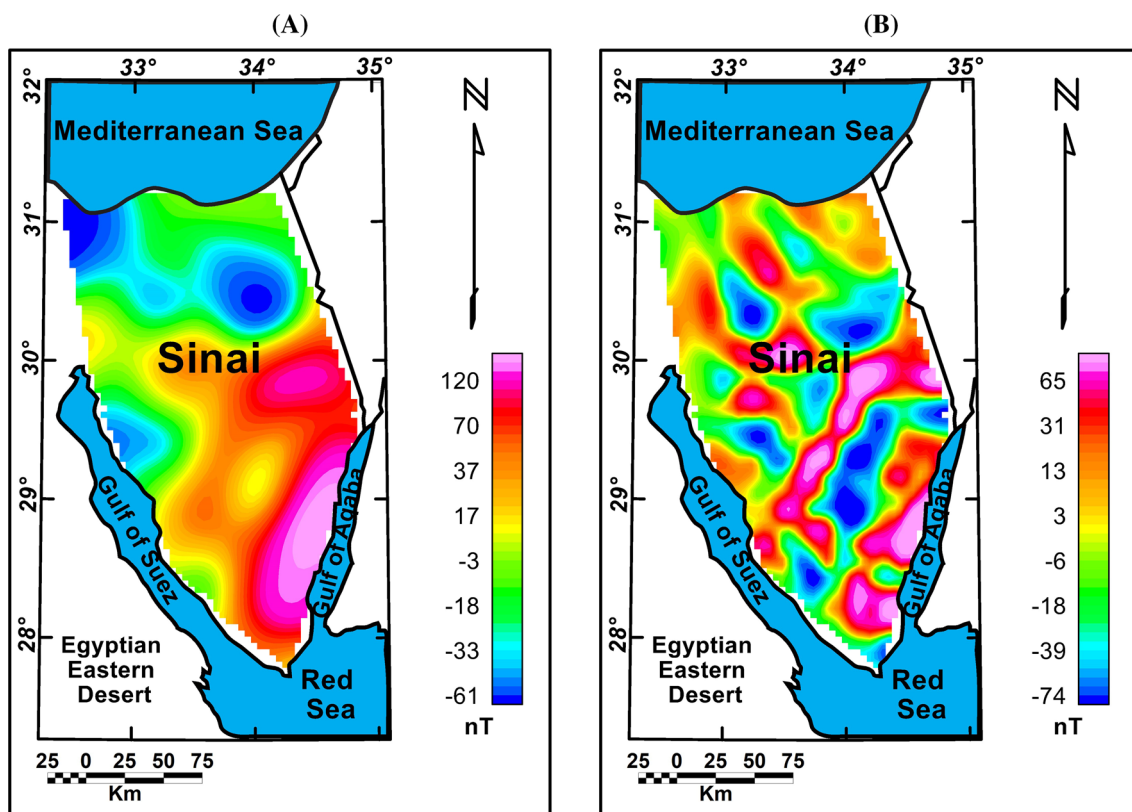


Fig. 8 Filtered RTP Aeromagnetic images. **A** Regional low-pass filter (cut-off wavenumber=0.01 cycle/km). **B** Residual high-pass filter (cut-off wavenumber=0.01 cycle/km)

enough to suggest changes in the mass distributions of the lower and upper mantle and the isostatic balance distributions (Tealeb and Riad 1986). The relation between gravitational anomalies, crustal thickness, and surface relief has been reported by many researchers (e.g., Pick et al. 1973; Riad et al. 1983; El-Khadragy et al. 2010). The initial models were created by detecting the basement surface, Conrad discontinuity, and Moho discontinuity with the general trend of data by fitting observed and calculated Bouguer data.

Seventeen profiles were selected to cover the entire study area (Fig. 13A). Profiles (*P1*, *P5*, *P6*, *P12*, *P15*, *P16*, and *P17*) are oriented toward E–W, profiles (*P4*, *P7*, *P8*, *P9*, *P11*, and *P13*) are oriented toward NE–SW, and profiles (*P2*, *P3*, *P10*, and *P14*) are oriented toward NW–SE. These profiles represent the thickness of sedimentary rock, which increases in the North direction, and the basement rocks are outcropped in the South of Sinai. Due to the lack of well data in the Sinai region, most of these profiles were obtained through the results of previous studies in the area. Therefore, previous works about crustal thickness of that region (El-Khadragy et al. 2014; El Sayed and Essam 2012; El Khrepy et al. 2016) were used as the reference depth points shown in Fig. 13B.

Figure 14 shows that the average density of the sedimentary cover is 2300 kg/m^3 (yellow); the density is 2800 kg/m^3 for the basement surface (purple), 3000 kg/m^3 for the Conrad surface (light blue), and 3300 kg/m^3 for the Moho surface (green). Table 1 shows the densities of the ground layers that were reported in previous studies and used for the 3D forward modeling in Sinai (Fig. 15).

The 3D model built from the seventeen 2D models is shown in Fig. 13A. Figure 14 shows examples of the 2D models (*P2*, *P3*, *P4*, *P7*, *P9*, and *P10*). These models represent the crustal model obtained via the observed (dots) and calculated (solid lines) data fitting, where x is the location of the reference depth points shown in Fig. 13B. The gained depth maps of the basement, Conrad, and Moho surfaces, which show the depth variation (attributed to the Sea level), are represented in Fig. 15. These modeling processes were followed by the generation of a 3D model of the upper crust, lower crust, and upper mantle (Fig. 16A). This 3D model may enable the extraction of any 2D profile along the study area, an example is illustrated in Fig. 16B. Figure 17 shows the gravity anomaly maps extracted from the 3D model and the residual map, which explains the quality of this model.

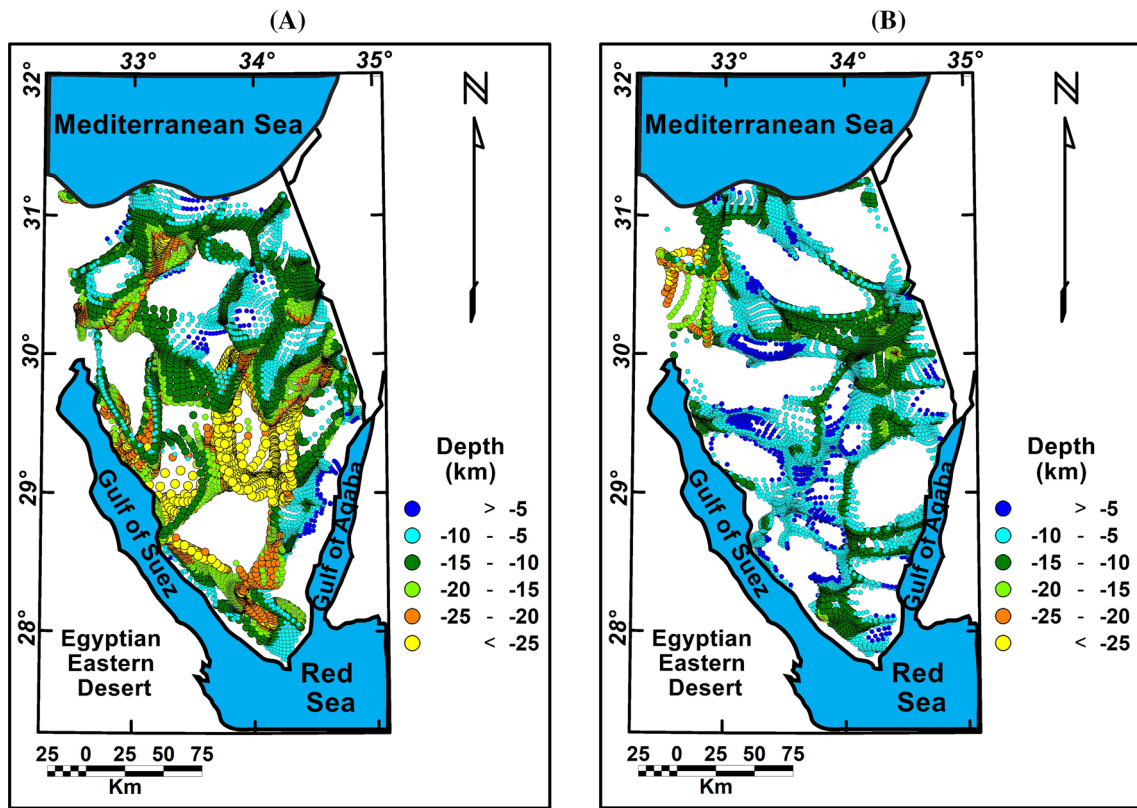
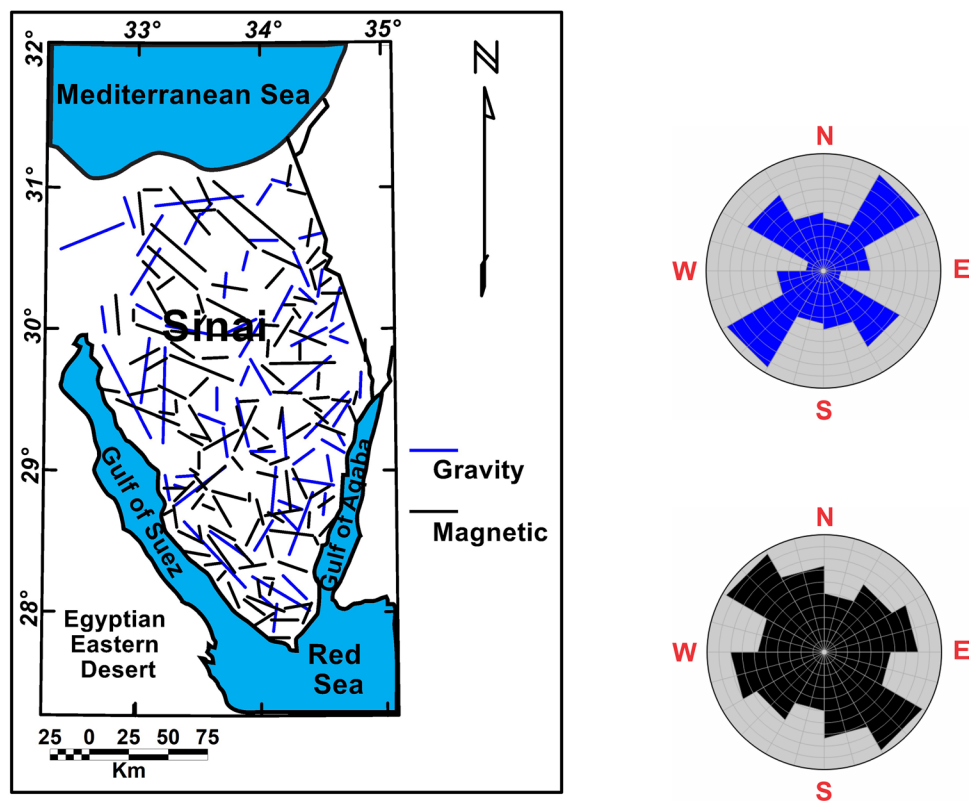


Fig. 9 3D Euler's solutions for **A** gravity data with (SI=1), and **B** RTP aeromagnetic data with (SI=0.5)

Fig. 10 Tentative basement structure map extracted by the 3D Euler's solutions from magnetic data (black lines) and from gravity data (blue lines), with a Rose diagram describing trends frequency



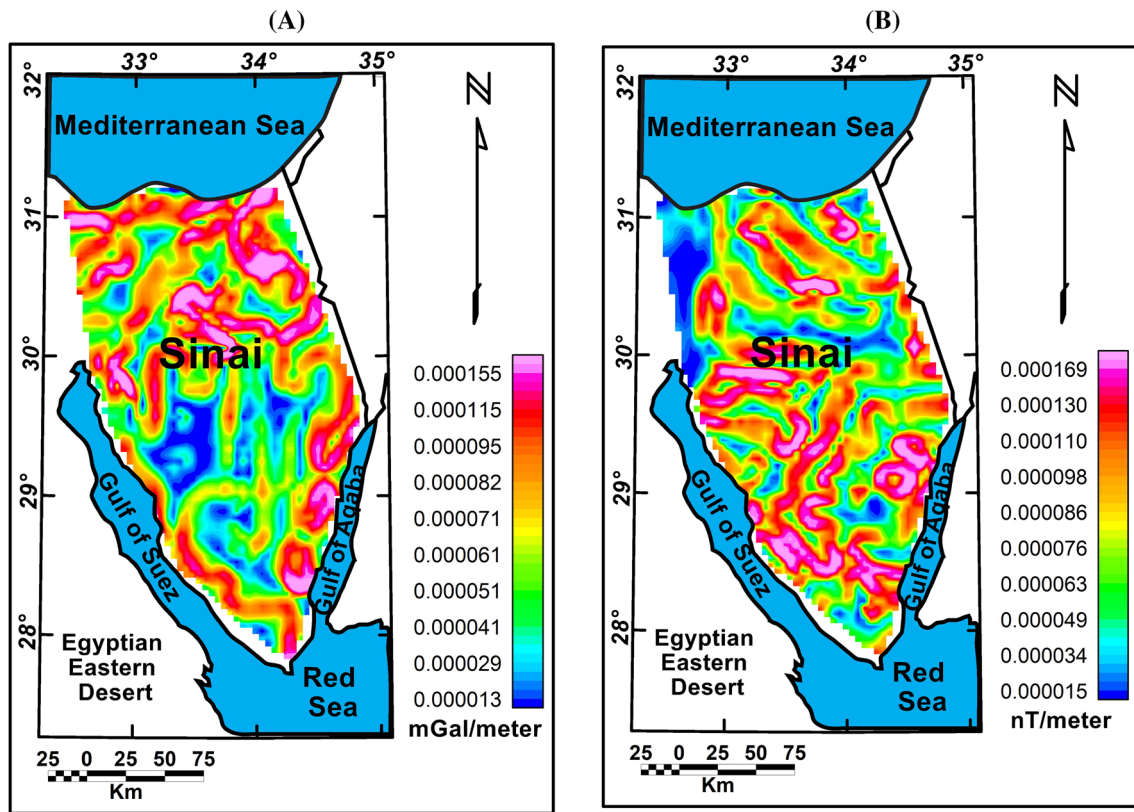
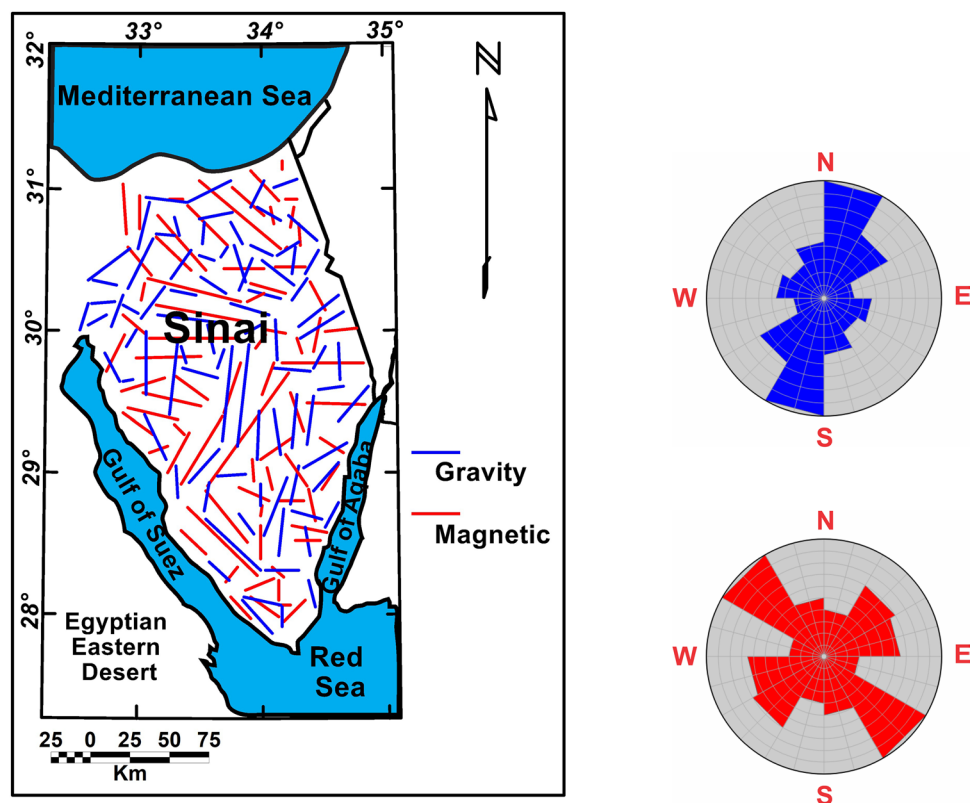


Fig. 11 The H-gradient maps for **A** Bouguer gravity data, and **B** RTP aeromagnetic data

Fig. 12 Tentative basement structure map constructed from the H-gradient filter of gravity data (blue lines) and magnetic data (red lines), with a Rose diagram describing trends frequency



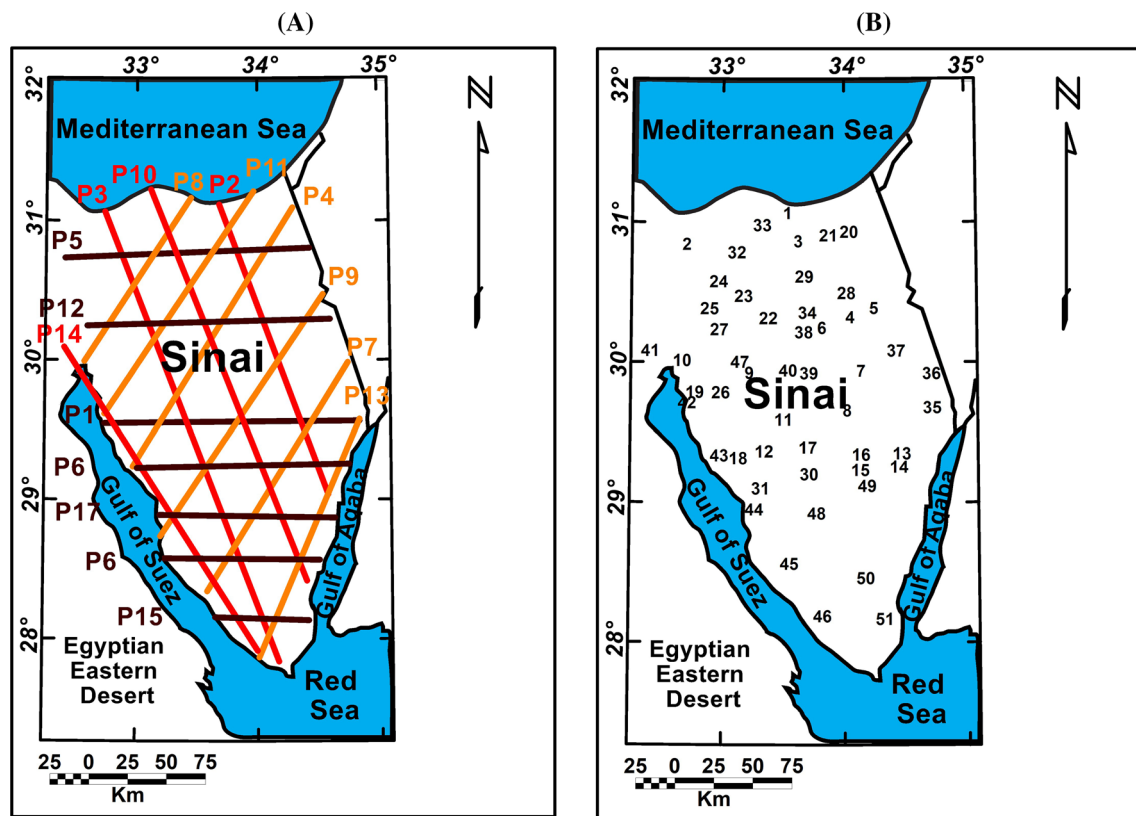


Fig. 13 **A** Locations of the profiles chosen for the 2D modeling of gravity data. E-W orientations are shown as brown lines, NW–SE orientations are shown as red lines, and NE–SW orientations are shown

as orange lines. **B** A base map showing locations of the crustal layer depth points takes from previous studies of (El-Khadragy et al. 2014; El Sayed and Essam 2012; El Khrepy et al. 2016)

Results and discussion

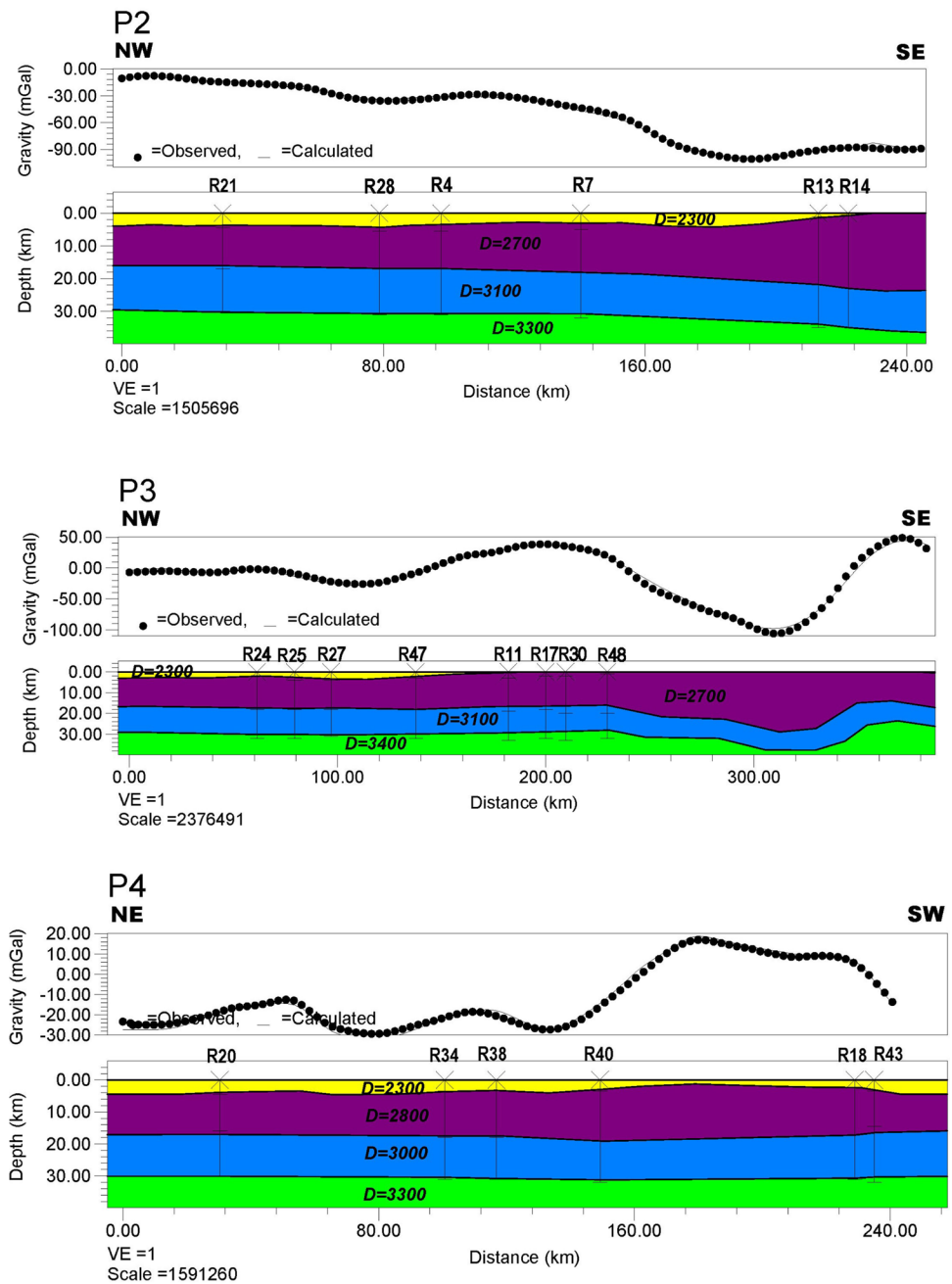
The distribution of earthquakes (Fig. 4) depicts the tectonic action in the Sinai Peninsula, with a high concentration in its southern portion parallel to the Gulf of Suez and the Gulf of Aqaba motions. According to the description of seismic source zones of Abdel-Rahman et al. (2009), the most active zones are the Aqaba (AQ) and the southern Gulf of Suez (SGZ). The crustal motions between the Arabian plate, African plate, and Sinai subplate result in a high seismicity rate in the SGZ zone. The high seismic activity of the AQ zone is attributed to the Gulf of Aqaba's left-lateral strike-slip movement (Ben-Avraham 1985; Toni 2012; Toni et al., 2016, 2019a, b; Badreldin et al. 2019; Hagag et al. 2019). Abdel-Rahman et al. (2009) reported that recent earthquakes all over the Sinai Peninsula are larger than historical ones, which agrees with the region's neotectonic reactivation models. The vertical distribution of the earthquake focal depths (Fig. 18) shows that the strongest earthquake motion occurs in the upper crust layer.

The major tectonic elements map (Fig. 19) derived in this study is based on the 3D Euler technique, the H-gradient filtering of Bouguer and RTP aeromagnetic data

(Figs. 10 and 12), and the major tectonic elements illustrated in Fig. 2. Analysis of the tectonic elements map (Fig. 19) demonstrates the following:

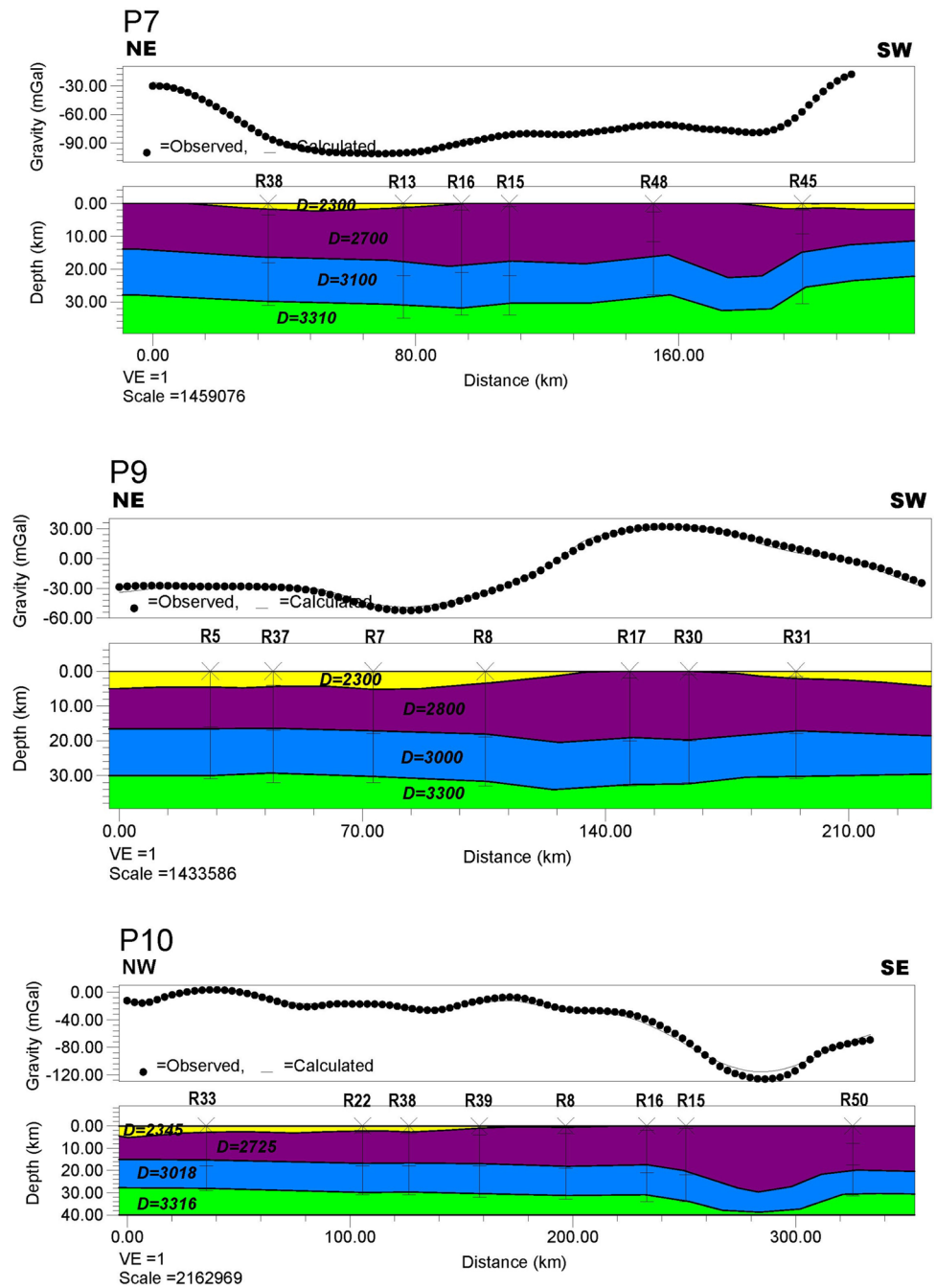
- (1) The Sinai area is covered by many synforms (depressions) and antiforms (uplifts) resulting from several intersection faults extending in the NE–SW, E–W, and NW–SE directions.
- (2) The study area's significant trends are E–W, NW–SE, and NE–SW from the major uplifts and basins that extend in the same directions. These trends appear in the northern and middle parts of Sinai (North Ragabet El-Naam shear zone) (Fig. 19).
- (3) The study region is influenced by various tectonic forces resulting in sets of structural contacts with different trends and magnitudes (Fig. 19).
- (4) In the NNW and NW directions, most of the contact and dyke solutions are related to the Red Sea trend. Solutions trend toward NE–SW in several locations of dykes and contacts (Fig. 19), and they are influenced by the transformed faults associated with the Red Sea rifting (Said 1962).

Fig. 14 A Examples of the gravity models profiles using reference depth's point shown in (Fig. 13B)



- (5) The NNW–SSE and NW–SE clustering of the obtained solutions shows prevailing deep structural patterns (orientation of the early Red Sea rift) that are influenced by extension and rifting processes. These patterns emerge progressively in the proto-Red Sea and are visible in the Arabian Peninsula (Richter et al. 1991).
- (6) Minor clustering solutions in the directions of E–W (Ragabet El-Naam fault system) and N–S (East African rift system) are visible on the magnetic Euler solution map. The Syrian Arc structural system is represented as E–W trending in central Sinai, while an N–S trend (East African rift system) is observed along with the central and southern parts of Sinai.
- (7) The Sinai Peninsula is a major tectonic province dominated by trends of the Red Sea, the Gulf of Suez, and the Gulf of Aqaba from a geologic and tectonic perspective (Abu El-Izz 1971; Toni et al. 2016; Badreldin et al. 2019).
- (8) Deep Euler contacts (20–25 km) trending in the NE–SW direction are observed in the northwestern part of Sinai; they coincide with the Moghara Mega shear fault system and are well comparable with that passing through the tip of the Suez rift, as discussed by Saleh

Fig. 14 (continued)

**Table 1** Values of density used for 3D forward modeling

Layer	Density (kg/m ³)	References
Sediments	2400	Ginzburg and Ben-Avraham (1987); Makris and Wang (1994)
Upper crust	2700	Ginzburg and Ben-Avraham (1987); Abdel-Rahman et al. (1988); Makris and Wang (1994)
Lower crust	2900	Jacobs et al. (1959); Makris et al. (1979); Ginzburg and Ben-Avraham (1987); Prodehl and Mechie (1991); Rihm et al. (1991); Makris and Wang (1994)
Upper mantle	3250–3300	Jacobs et al. (1959); Ginzburg and Ben-Avraham (1987); Makris and Wang (1994)

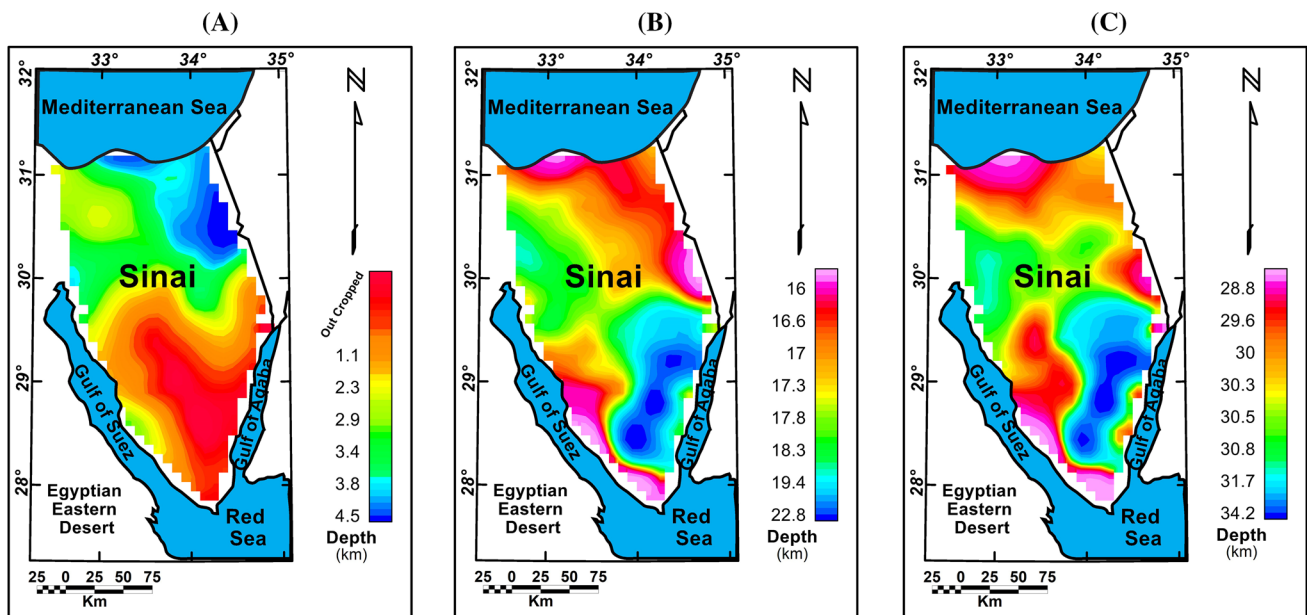


Fig. 15 **A** Basement surface, **B** Conrad surface, and **C** Moho surface depth maps of the Sinai Peninsula extracted from the 3D gravity model

and Pašteka (2012). These deep contacts (Fig. 9A) mostly reach the boundary between the Conrad and Moho discontinuities.

- (9) In the southern part of Sinai, the structural elements form a significant uplift that extends along the southeastern part of the area (southeast Ragabet El-Naam shear zone, Fig. 19). This uplift is observed in Fig. 15A, where the sedimentary cover reaches its minimum value.
- (10) There are two major strike-slip faults in the central part of Sinai with left and right lateral movements, Fig. 19.

The 3D model displays the basement, Conrad, and Moho surfaces (Figs. 15 and 16A). The estimated basement depth map shows that the sedimentary cover thickness increases in the North and decreases in the southeast of Sinai (Fig. 15A). Significant fault zones that are often in the E–W, NE–SW, and NW–SE directions control alternative depressions and uplifts. The thickness of the sedimentary cover ranges from 3.4 to 4.5 km in the northern part of Sinai, and the basement reaches the surface in the southeastern part. The highly elevated area in the northwestern part (intersection of N 30° 00' and E 33° 30') is a North Sinai ridge that represents an uplifted ENE-trending basement structure (Fig. 15A). The oldest structures (most likely Paleozoic to Triassic) trend toward NW or WNW, followed by another event (most likely Cretaceous) in the ENE (Syrian Arc) trending structures. The E–W, NW, and NNE trending systems were formed by the last tectonic event, which most likely occurred in the late Eocene to early Oligocene (Saad et al. 2010).

The Conrad surface map (Fig. 15B) shows a decrease in its depth in the NE–SW direction. The depth to the Conrad varies from 16 km (in the northeastern and southwestern parts of Sinai) to 22.8 km (in the southeast). The depth to the Moho surface (Fig. 15C) ranges between 28.8 and 34.2 km, and it deepens in the northeastern and southwestern parts of Sinai. Table 2 displays a comparison between the depths of the basement, Conrad, and Moho surfaces estimated in the present study and those estimated in previous studies.

Table 2 shows that the present results lie within the range of the previous findings. The extensive range of our results may be because of the expansion of the Sinai Peninsula, with a sharp variation in depth between the North and South. There is a rapid change in the Conrad and Moho depths in the North and near the Mediterranean with a decrease in the crustal thickness. The northward decrease in the Moho and Conrad depths indicates a transition zone between the continental and oceanic crusts.

The gravity anomaly maps (observed, calculated, and residual, Fig. 17), which validate the quality of this forward model, cover the entire Sinai area with accurate details and the ability to extract any 2D model along the area.

The map of major tectonic elements (Fig. 19) was compiled from: (1) Tentative basement maps extracted from the H-gradient and the 3D Euler techniques (Figs. 10 and 12) and (2) Major tectonic elements map (Fig. 2). The findings of the tectonic evaluation indicate that the Sinai region is influenced by six tectonic trends: NNE (Aqaba), NW (Suez), ENE (Syrian Arc), WNW (Najd), E–W (Tethyan), and N–S (North Sinai and East African). A strike-slip fault with vertical and horizontal movements in the center of Sinai divides

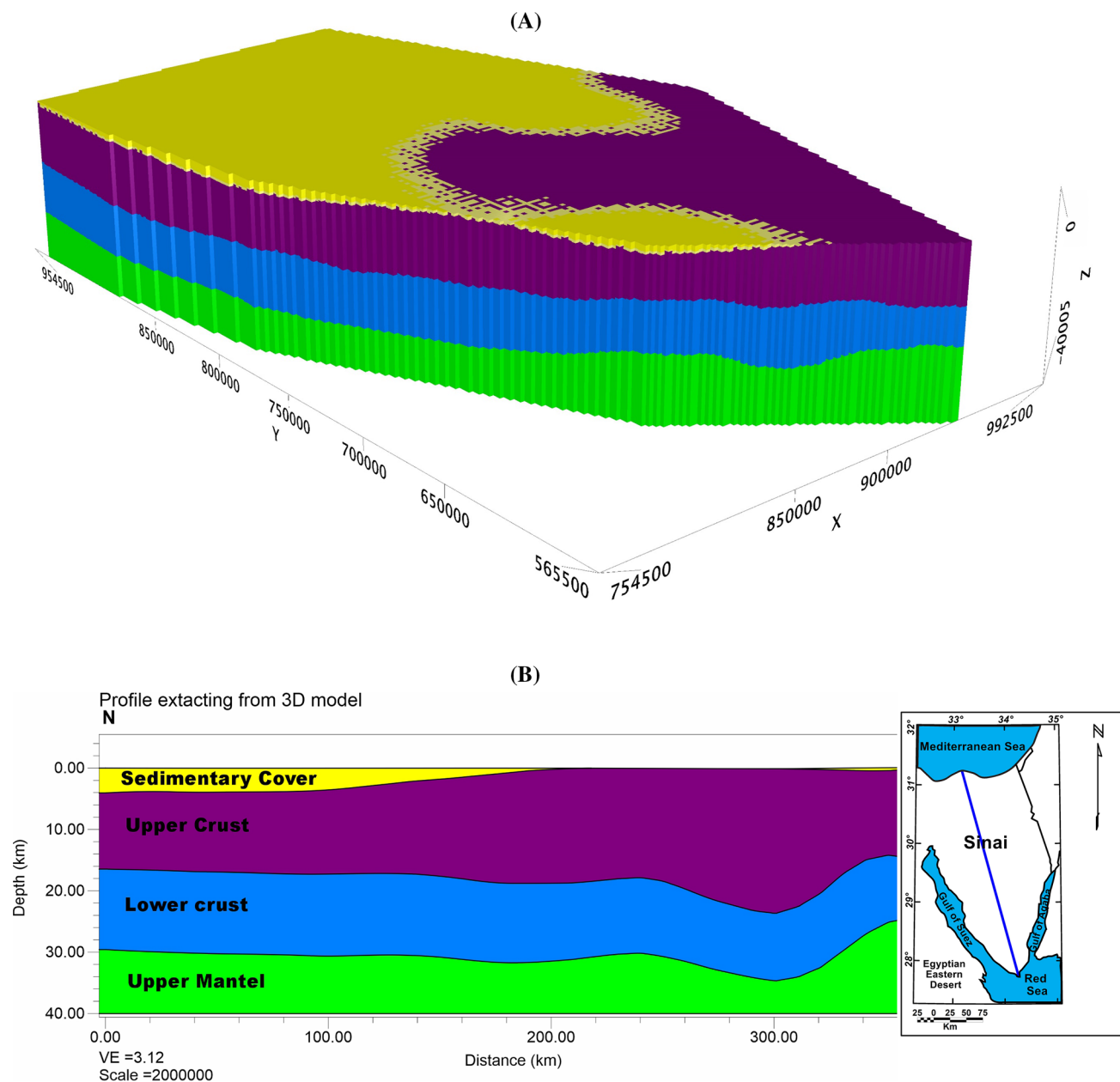


Fig. 16 **A** 3D modeling of the crustal structure (sedimentary cover, upper and lower Crust, and upper Mantel) in the Sinai Peninsula. **B** An example of the gravity models in the N-S direction extracted from a 3D model

the peninsula into two parts. The *northern part* (North Ragabet El-Naam shear zone, Fig. 19) has a principal tectonic trend oriented in the NE–SW direction; it is affected by the Mesozoic compression of the Syrian Arc system and the structure inverted to old extensional basins formed during the Jurassic and Early Cretaceous opening (Said 1990). The *southern part* (South Ragabet El-Naam shear zone, Fig. 19) has a principal tectonic trend oriented in the NE–SW direction and connected to the NW–SE tectonic trend of the Syrian Arc, and it is the second predominant order. This trend originates from the Gulf of Suez opening and is normal to

the NE–SW tension axis (Said 1990). The established N–S and NW–SE tectonic patterns related to the Gulf of Aqaba may be the third dominant order.

Conclusions

The results obtained from Bouguer gravity data, RTP aeromagnetic data, seismicity data, 3D gravity model, and a tentative basement structural map enabled us to generate the following conclusions:

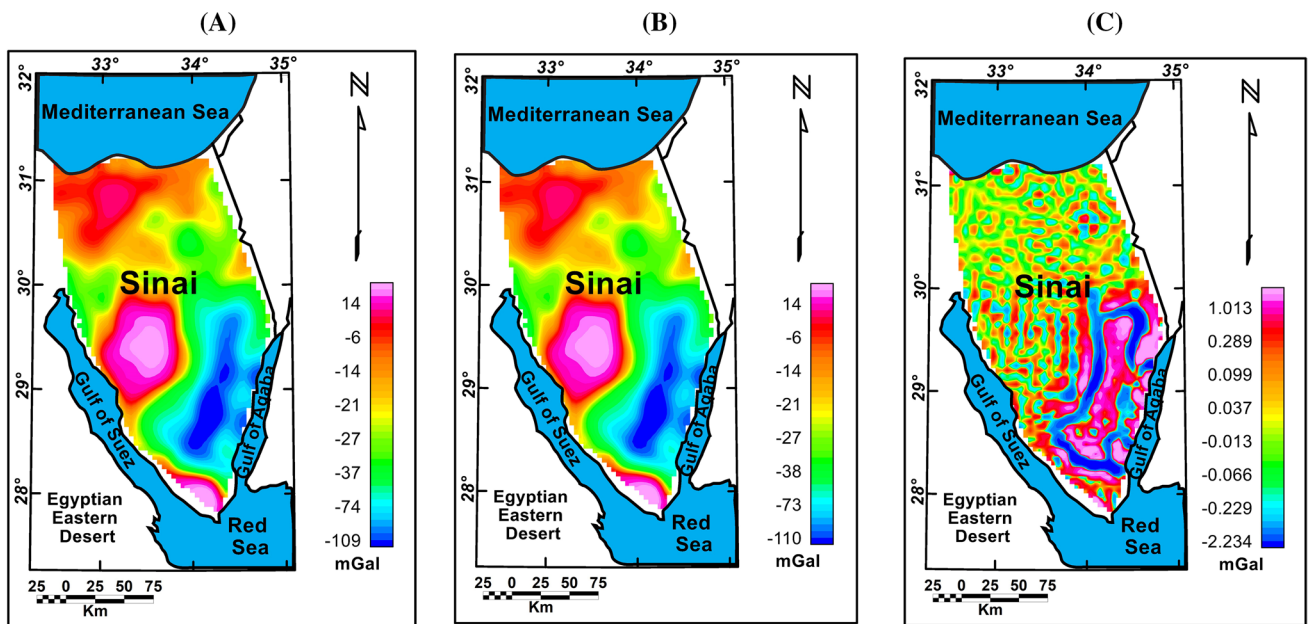


Fig. 17 A Observed, B Calculated, and C Residual anomaly maps of the Sinai Peninsula resulted from the 3D gravity model

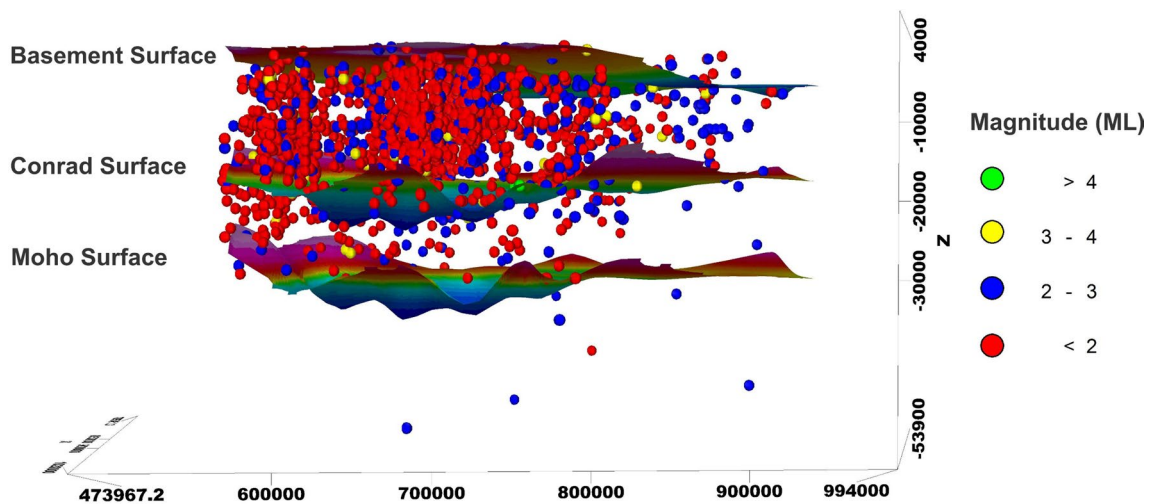


Fig. 18 3D view from 3D modeling of the crustal structure of the Sinai Peninsula with the vertical distribution of earthquakes' focal depths

1. The basement surface shapes of the anomalies and trends were determined from the regional RTP aeromagnetic map. The basement surface in the Sinai Peninsula is not flat, and the basement depth varies from the outcropped surface to 4.5 km. In general, the depth to the basement surface increases in the North direction.
2. The Conrad discontinuity occurs at a depth of 16–22.8 km and shows a strong variation in its relief. The Moho discontinuity, which can determine anomalies, shapes, and trends from the regional Bouguer gravity map, occurs at a depth of 28.8–34.2 km. The Conrad

and Moho discontinuities are almost parallel and slope off to the southeast.

3. The study area has a typical continental crustal type, and its thickness decreases northward and increases southeastward. The overlying sedimentary layer becomes dense in the northward direction.

4. A high-resolution 3D forward model with a small error was constructed for the study area. The ability to collect 2D profiles at any position within the Sinai region and calculate the depths of basement, Conrad, and Moho surfaces with high resolution makes the pre-

Fig. 19 Modified tectonic elements of the Sinai Peninsula compiled between tentative basement map extracted from the H-gradient and 3D Euler’s solution, and the structural map of Neev (1975). The new fractures are added in orange color

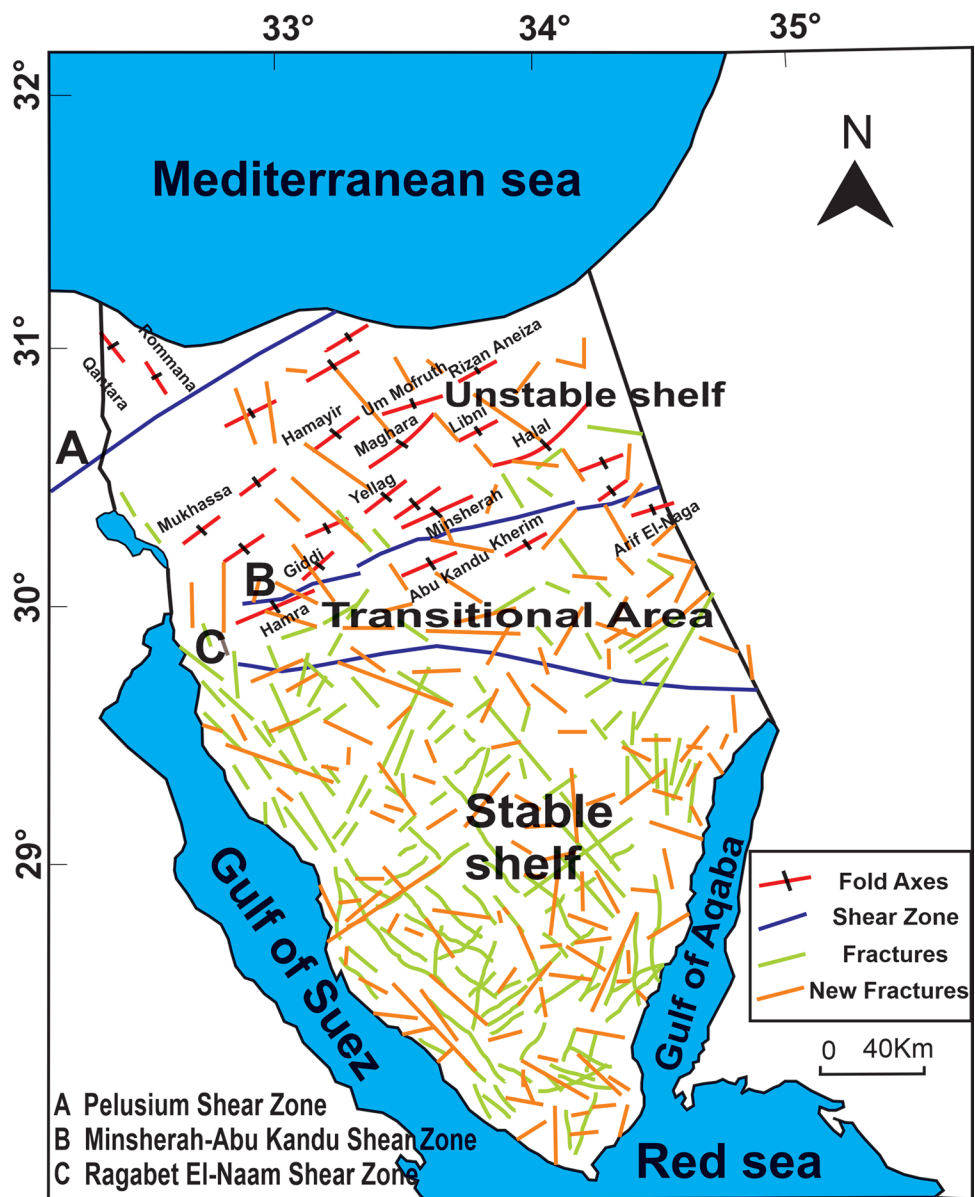


Table 2 Estimated depths in Sinai Peninsula

References	Used method	Depth (km)		
		Basement	Conrad	Moho
Present study	Gravity	Outcropped–4.5	16–22.8	28.8–34.2
Corchete et al. (2017)	Rayleigh wave analysis	None	None	30–35
Hosny and Nyblade (2016)	Receiver functions	None	None	32–38
Abdelwahed et al. (2013)	Local earthquake travel time inversion	None	14–15	31–35
El-Khadragy et al. (2010)	Gravity + seismic	2.5–5.5	19.5–22.7	32–35
Saleh et al. (2006)	Gravity	None	None	31
Dorre et al. (1997)	Gravity	None	None	32–34
Marzouk (1988)	Seismic profiles	None	19–22	31–33
Makris et al. (1988)	Seismic profiles	None	None	28–35
Ginzburg et al. (1981)	Deep seismic sounding	None	None	33–35

sent study useful for future geophysical and geological investigations.

5. The relative motions along the Gulf of Aqaba and the Gulf of Suez make the South Sinai area tectonically active. The crust layer of the Sinai Peninsula experiences massive tectonic motions. Furthermore, neotectonic reactivation models can be seen in the distribution of earthquakes over the region.

6. The basement structural configuration in Sinai is distinguished by uplifts and basins, where the thickness of the sedimentary cover varies. Two main trends in the tentative basement structural map influence the study area; the NE–SW and NW–SE fault trends are intersected by the E–W transform faults in central Sinai. These trends are believed to have resulted from two maximum principal stresses oriented toward N–S and NNW–SSE. Northern Sinai is structurally associated with the Syrian Arc and the Mediterranean trends. Meanwhile, Southern Sinai is mainly dominated by the rifting and developing the Gulf of Suez and the Gulf of Aqaba.

This study is useful for other researchers who want to verify whether the Sinai Peninsula is an individual subplate with its own movement. The events that occurred between the Afro-Arabian and Eurasian plates (Syrian Arc) and the movement that occurred along the Gulf of Suez and the Gulf of Aqaba control the structure of Sinai Peninsula. Furthermore, the southern part of Sinai is more active and developed than the northern part.

Acknowledgements The geophysical data was supported by NRIAG, Egypt. The English proofreading was covered by the Egyptian Knowledge Bank (EKB), and grammar, punctuation, and spelling have been checked by ENAGO Language editing services (www.enago.com). The authors greatly appreciate Mr. Ahmed Mohammed Ibrahim from Bahrain Ministry of Education (BH MOE) for the fine revision of the language of this article.

Funding Open access funding provided by The Science, Technology & Innovation Funding Authority (STDF) in cooperation with The Egyptian Knowledge Bank (EKB).

Declarations

Conflict of interest The authors declare that they have no known competing financial interests or personal relationships that could have appeared to influence the work reported in this paper.

Open Access This article is licensed under a Creative Commons Attribution 4.0 International License, which permits use, sharing, adaptation, distribution and reproduction in any medium or format, as long as you give appropriate credit to the original author(s) and the source, provide a link to the Creative Commons licence, and indicate if changes were made. The images or other third party material in this article are included in the article's Creative Commons licence, unless indicated otherwise in a credit line to the material. If material is not included in the article's Creative Commons licence and your intended use is not

permitted by statutory regulation or exceeds the permitted use, you will need to obtain permission directly from the copyright holder. To view a copy of this licence, visit <http://creativecommons.org/licenses/by/4.0/>.

References

- Abdel-Rahman K, Al-Amri AMS, Abdel-Moneim E (2009) Seismicity of Sinai Peninsula, Egypt. *Arab J Geosci* 2:103
- Abdelrahman E, Refai E, El-Ghalban H (1988) Gravity models of the Nile delta basin Egypt. In: *Egyptian geological survey proceedings of 6th annual meeting*, pp 33
- Abdelwahed MF, El-Khrepy S, Qaddah A (2013) Three-dimensional structure of Conrad and Moho discontinuities in Egypt. *J Afr Earth Sci* 85:87–102
- Abu El-Ata ASA, Rizkalla RI, Abdel Hady AI (1991) The role of wave number filtering in the separation of the residual and regional gravity anomalies of northwestern Sinai Peninsula. In: *Egypt proceedings of the 9th annual meeting*, pp 19–42
- Abu El-Izz MS (1971) *Landforms of Egypt*. American University of Cairo Press, Dar Al-Maaref, Cairo
- Badreldin H, Abd el-aal AK, Toni M, El-Faragawy K (2019) Moment tensor inversion of small-to-moderate size local earthquakes in Egypt. *J African Earth Sci* 151:153–172. <https://doi.org/10.1016/j.jafrearsci.2018.12.004>
- Ben-Avraham Z (1985) Structural framework of the Gulf of Aqaba, northern Red Sea. *J Geophys Res* 90:703–726
- Bhattacharyya B (1965) Two-dimensional harmonic analysis as a tool for magnetic interpretation. *Geophysics* 30(5):829–857
- Corchete V, Chourak M, Hussein H, Atiya K, Timoulali Y (2017) Crustal and upper mantle structure of the north-east of Egypt and the Afro-Arabian plate boundary region from Rayleigh-wave analysis. *J Afr Earth Sci* 129:195–201
- Dorre AS, Carrara E, Cella F, Grimaldi M, Hady YA, Hassan H, Rapolla A, Roberti N (1997) Crustal thickness of Egypt determined by gravity data. *J Afr Earth Sci* 25:425–434
- EGPC (1985) Bouguer gravity anomaly map for Sinai Peninsula (scale 1:100 000). Egyptian General Petroleum Corporation (EGPC)
- EGPC (1990) Aeromagnetic map for Sinai Peninsula (scale 1:100 000). Egyptian General Petroleum Corporation (EGPC)
- El Sayed S, Essam A (2012) Determination of sedimentary cover and structural trends in the central Sinai area using gravity and magnetic data analysis. *J Asian Earth Sci* 43:193–206
- El Khrepy S, Koulakov I, Al-Arifi N (2016) Crustal and uppermost mantle structure beneath the continental rifting area of the Gulf of Suez from earthquake tomography. *Tectonophysics* 668–669:92–104
- El Nashar ER, El-Omla MM, Abd El-Shakour ZA (2012) Petrographical and geochemical characteristics of north Ras Mohamed granitic rocks, southern Sinai, Egypt. *Egypt J Geol* 56:411–431
- El-Kerdany M (1962) *General study on North Sinai, Egypt*. G.P.C., vol 210, Egypt
- El-Khadragy AA, Saad MH, Azab A (2010) Crustal modelling of South Sitra area, North western Desert, Egypt using Bouguer gravity data. *J Appl Sci Res* 6(1):22–37
- El-Khadragy AA, Azab AA, El-Khateef A (2014) Contribution to the integrated interpretation of gravity, aeromagnetic and seismic data of the northern and central parts of Sinai, Egypt. *World Appl Sci J* 31(9):1540–1551
- Eweis AM, Toni M, Basheer AA (2021) Depicting the main structural affected trends by operating aeromagnetic survey in the western part of Koraimat-Alzafarana road and surround area, Eastern Desert, Egypt. *Model Earth Syst Environ*. <https://doi.org/10.1007/s40808-021-01265-7>

- Ghoneim MF, Heikal MThS, El Dosuky BT, Abu-Alam TS, Sherif MI (2015) Neoproterozoic granites of Sharm El-Sheikh area, Egypt: mineralogical and thermobarometric variations. *Arab J Geosci* 8:125–141
- Ginzburg A, Makris J, Fuchs K, Prodehl C (1981) The structure of the crust and upper mantle in the dead sea rift. *Tectonophysics* 80:109–119
- Ginzburg A, Ben-Avraham Z (1987) The deep structure of the central and southern levant continental margin. *Ann Tecton*, pp 105–115
- Hagag W, Hassan S, Toni M (2019) Active tectonic structures in north-eastern Egypt: a geospatial analysis using structural, remote sensing, and seismic data. *Arab J Geosci* 12(18):1–16. <https://doi.org/10.1007/s12517-019-4749-6>
- Hosny A, Nyblade A (2016) The crustal structure of Egypt and the northern red sea region. *Tectonophysics* 687:257–267
- Jacobs J, Russell R, Wilson J (1959) *Physics and geology*. McGraw-Hill, New York
- Khalaf IM, Ahmed AM, Seweifi BM (1994) The granitoids of Ras Muhammad area, south Sinai, Egypt. *Egypt J Geol* 38:125–139
- Kora M (1995) An introduction to the stratigraphy of Egypt. Lecture notes, Department Of Geology, Mansoura University, Egypt, p 116
- Makris J, Stofen B, Veas R, Allam A, Maamoun M, Shehata W (1979) Deep seismic sounding in Egypt, part I: the Mediterranean Sea between Crete, Sidi Barani, and the coastal area of Egypt. Unpublished report, National Research Institute of Astronomy and Geophysics, Helwan, Egypt
- Makris J, Wang J (1994) Bouguer gravity anomalies of the eastern Mediterranean Sea. In: Krasheninnikov VH (ed) *Geological structure of the northeastern mediterranean (Cruise 5 of the Research Vessel "Akademik Nikolaj Strakhov")*. Historical Production Hall Ltd, Jerusalem, pp 87–98
- Makris J, Rihm R, Allam A (1988) Some geophysical aspects of the evolution and structure of the crust in Egypt. In: Greiling S-G (ed) *The Pan-African belt of Northeast Africa and adjacent areas, tectonic evolution and economic aspects of a late proterozoic Orogen* Vieweg & Sohn, Braunschweig, Friedr, pp 345–369
- Marzouk I (1988) Study of crustal structure of Egypt deduced from deep seismic and gravity data Ph.D thesis 188. University of Hamburg, W. Germany
- Meshref W, Hammouda H (1990) Basement tectonic map of northern Egypt. 10th Exploration production conference, EGPC, Cairo, p 23
- Meshref W (1989) Energy resources in Sinai. In: *Proceeding 2nd conference geology Sinai, Ismailia*, pp 142–152
- Mohamed H, Senosy M, Abdel Zaher M (2016) Interactive interpretation of airborne gravity, magnetic, and drill-hole data within the crustal framework of the northern Western Desert, Egypt. *J Appl Geophys* 134:291–301
- Moustafa A R, Khalil M H (1987). North Sinai structures and tectonic evolution. In: 25th annual Meeting, Geological Society of Egypt, pp 3–4
- Moustafa AR, Khalil MH (1990) Structural characteristic and tectonic evaluation. In: Said R (ed) *Geology of Egypt*, vol 743. Balkman Publ, London, pp 381–389
- Neev D (1975) Tectonic evolution of the middle east and levantine basin (Easternmost Mediterranean). *Geology* 3:683–686
- Neev D, Almador G, Arad A, Ginzburg A, Hall JK (1973) The geology of the southeastern Mediterranean Sea. *Geological Survey of Israel Rep. M.G./73/5*, pp 43
- Omara S (1972) An early Cambrian outcrop in southwestern Sinai, Egypt. *N JP Geol Palaeontol* 5:306–314
- Pick M, Picha J, Vyskocil V (1973) *Theory of the earth's gravity field*. Academia, Prague, p 538
- Prodehl C, Mechie J (1991) Crustal thinning in relationship to the evolution of the afro-Arabian rift system: a review of seismic-refraction data. *Tectonophysics* 198:311–327
- Reid AB, Allsop JM, Granser H, Millett AJ, Somerton IW (1990) Magnetic interpretation in three dimensions using Euler deconvolution. *Geophysics* 55:80–90
- Riad S, Fouad A, Refai E, Ghalib M (1983) Preliminary interpretation of regional gravity anomalies of Egypt. IUGG Inter-disciplinary symposium Hamburg
- Richter H, Makris J, Rihm R (1991) Geophysical observations offshore Saudi Arabia: seismic and magnetic measurements. *Tectonophysics* 198:297–310
- Rihm R, Makris J, Moller L (1991) Seismic surveys in the northern red sea: asymmetric crustal structure. *Tectonophysics* 198:279–295
- Saad M, El-Gezeery R, El-Khateef A (2010) Delineating the subsurface structural setting of the northwestern part of Sinai Peninsula using aeromagnetic and gravity data. *J Appl Sci Res* 6(9):1412–1430
- Said R (1962) *The geology of Egypt*. Elsevier, Amsterdam
- Said R (1990) *The geology of Egypt*, 2nd edn. Balkema, Rotterdam
- Saleh S, Jahr T, Jentzsch G, Saleh A, Ashour NA (2006) Crustal evaluation of the northern red sea rift and gulf of Suez, Egypt from geophysical data: 3-dimensional modelling. *J Afr Earth Sci* 45:257–278
- Saleh S, Pašteka R (2012) Applying the regularised derivatives approach in Euler deconvolution and modeling geophysical data to estimate the deep active structures for the northern Red Sea Rift region, Egypt. *Contrib Geophys Geod* 42(1):25–61
- Salem A, Williams S, Fairhead D, Smith R, Ravat D (2008) Interpretation of magnetic data using tilt angle derivatives. *Geophysics* 73:L1–L9
- Shata A (1955) Some remarks on the distribution of the carboniferous formation in. *Inst Desert Egypt* 5:241–262
- Shata A (1956) Structure development of Sinai Peninsula, Egypt. *Bull Inst Desert Egypt* 6:117–157
- Sherif MI, Ghoneim MF, Heikal MTSE, Dosuky BT (2013) Petrogenesis of granites, Sharm El-Sheikh area, South Sinai, Egypt: petrological constraints and tectonic evolution. *Miner Pet* 107:765–783
- Tealeb A, Riad S (1986) Regional gravity anomalies of western Saudi Arabia and their geological significance. In: *E G S Proceedings of 5th Annual Meeting, March 29–30*, pp 50–89
- Thompson D (1982) EULDPH- a new technique for making computer-assisted depth estimates from magnetic data. *Geophysics* 47:31–37
- Toni M, Barth A, Ali SM, Wenzel F (2016) Analysis of the similar epicenter earthquakes on 22 January 2013 and 01 June 2013, central gulf of Suez, Egypt. *J Afr Earth Sci* 121:274–285. <https://doi.org/10.1016/j.jafrearsci.2016.06.013>
- Toni M, Yokoi T, El Rayess M (2019a) Site characterization using passive seismic techniques: a case of Suez city, Egypt. *J Afr Earth Sci* 156:1–11. <https://doi.org/10.1016/j.jafrearsci.2019.05.004>
- Toni M, Yokoi T, El Rayess M (2019b) Determination of shallow site dynamic characteristics using seismic techniques in Suez city, Egypt. In: *Geophysical research abstracts*, vol 21, EGU General Assembly 2019b, 07–12 Apr. 2019b, Vienna, Austria
- Toni M (2012) Site response and seismic hazard assessment for the southern part of Cairo City, Egypt. Ph.D. Dissertation, Faculty of Science, Assiut University, Egypt